International Journal of Biological Macromolecules 281 (2024) 136429

Contents lists available at ScienceDirect

International Journal of Biological Macromolecules

journal homepage: www.elsevier.com/locate/ijbiomac

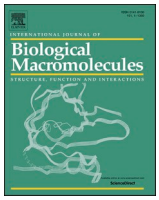

Structure formation mechanism of pectin-soy protein isolate gels: Unraveling the role of peach pectin fractions

Jin Xie [a,b], Jinfeng Bi [a,*], Nicolas Jacquet [b], Christophe Blecker [b], Shuhan Feng [c], Xiaoxian Liu [b], Jian Lyu [a,*]

[a] Institute of Food Science and Technology, Chinese Academy of Agricultural Sciences, Key Laboratory of Agro-products Processing, Ministry of Agriculture and Rural Affairs, Beijing 100193, China
[b] University of Liège, Gembloux Agro-Bio Tech, Unit of Food Science and Formulation, Avenue de la Faculté d'Agronomie 2B, Gembloux B-5030, Belgium
[c] University of Helsinki, Drug Research Program, Division of Pharmaceutical Chemistry and Technology, Faculty of Pharmacy and Helsinki Insititute of Life Science, FI-00014 Helsinki, Finland

ARTICLE INFO

Keywords:
Peach pectin
Soy protein isolate
Rheological property
SEM-dispersive X-ray spectroscopy
Chemical force
NMR spectra

ABSTRACT

This study investigated the macro & micro properties of the composite gels formed by soy protein isolate (SPI) and peach pectin fractions: water-soluble pectin (WSP), chelator-soluble pectin (CSP), and sodium carbonate soluble pectin (NSP). Specially, the interaction between pectin fractions and SPI was studied to explain the formation mechanism of the composite gels. WSP, as a high methoxyl pectin, exhibited rich branching (sugar ratio B = 3.10). CSP, as a low methoxyl pectin, depicted a high linearity. NSP, with low linearity (sugar ratio A = 6.14), contained numerous side chains. Due to the strong interaction between pectin fractions and SPI, the new composites with excellent dense network microstructures were formed, accompanied by increased apparent viscosity, higher G′ and G″, and reduced particle size. XRD and FT-IR analysis highlighted the modifications in gel structures. SEM-dispersive X-ray spectroscopy observed elemental distribution and framework composition in pectin-SPI gels. Hydrophobic interaction was the most important chemical force in pectin-SPI binding. Molecular docking results indicated that galacturonic acid in pectin bound more strongly to 7S than to 11S, with tighter hydrogen bonds. Notably, WSP-SPI showed the lowest turbidity, indicating enhanced solubility and particle dispersion, which helped prevent aggregation. CSP-SPI demonstrated the highest G′ and G″, ascribing to the high linearity and abundant carboxyl groups in CSP. NSP-SPI showed the highest apparent viscosity and irregular structure. Overall, the texture properties of pectin-SPI gels were driven by pectin's structure properties, which would provide new and valuable information for texture control in gel formulation.

1. Introduction

Pectin, a complex group of polysaccharides presented in high plant tissues, has garnered significant attention in the food industry to alter food texture, owing to its unique gelation properties [1,2]. Generally, homogalacturonan (HG), rhamnogalacturonan I (RG-I), and rhamnogalacturonan II (RG-II) are considered as the main three primary regions in pectin structure [3]. HG consists of α (1 → 4) linked D-galacturonic acid units, with several C-6 carboxyl groups undergoing methyl esterification, which is known as the "smooth region" of pectin [4]. RG-I and RG-II represent branched pectin polysaccharides with various side chains, constituting the "hairy region" of pectin. Additionally, based on the extraction methods and cross-linkages, pectin molecule is classified into three fractions: water-soluble pectin (WSP), chelator soluble pectin (CSP) and sodium carbonate soluble pectin (NSP). In detail, WSP is associated with cell wall by non-covalent bounds and non-ionic bonds, which mainly occur in branch chain of pectin. CSP, as the high linearity pectin, is predominantly consisting of ionically cross-linked pectin. NSP is primarily associated with cell-wall polysaccharides by covalent ester bonds [3]. As our previous study, the molecular weight (MW) of WSP inversely affected the hardness of yellow peach slices, whereas the degree of methoxylation (DM) in WSP directly enhanced the texture properties, such as chewiness, cohesiveness, resilience, and springiness. However, for both CSP and NSP, an increase in MW corresponded with great hardness, chewiness, and cohesiveness of yellow peaches [5]. Moreover, a negative correlation was observed between the hardness

* Corresponding authors.
E-mail addresses: bjfcaas@126.com (J. Bi), lvjianlinjian@163.com (J. Lyu).

https://doi.org/10.1016/j.ijbiomac.2024.136429
Received 19 July 2024; Received in revised form 2 October 2024; Accepted 7 October 2024
Available online 31 October 2024

and the galacturonic acid (GalA) content of WSP, which has been reported in grapes, dates, and apples [6,7]. It was reasonable to conclude that the structural attributes of pectin could affect the textural properties of compound food, which was crucial for innovation in food products [8,9].

Proteins, as the essential component of all living cells and tissues play an important role in human body. Additionally, the texture-customizable protein products with high quality can be considered as the solution for people who have difficulty in chewing or swallowing [10]. Soy protein isolate (SPI), known for its excellent foaming, emulsifying and gelling properties, has been widely used as an ingredient in various complex food systems [11]. Protein and pectin as natural macromolecules have been widely applied in food systems. Due to the interaction between pectin and protein, the phase behavior of pectin-protein complexes determines the physicochemical properties and macro- & micro- texture characteristics of the resulting polymers. Nowadays, growing investigations focus on the macro-properties of compound food from pectin and protein, particularly concerning mouthfeel. The electrostatic, hydrophobic, hydrogen bond and van der Waals force might be the main chemical force for the formation of protein-pectin composite [12]. The addition of pectin not only improves the gel strength of pectin-soy protein composites but also significantly enhances the storage modulus (G′), leading to a stable and densely meshed structure through an electrostatic effect [13]. The formation of a new network structure in pea protein isolate-high methoxyl pectin (HMP) composite supported the increased viscosity and the facilitated thermal denaturation temperature of the soluble complexes [14]. As for soy protein-pectin complexes, HMP facilitated soy protein aggregation and reduced gel strength, while low methoxyl pectin (LMP) with rich free carboxyl groups improved gel strength through electrostatic interactions [15]. Therefore, to explore the formation mechanism of pectin-protein compound, it was important to analyze the molecular structure, weight and composition of pectin polysaccharide and the interactions between pectin and proteins within the compound food system, which would provide new information for selecting the most suitable type of polysaccharide for the particular food formulation.

In this study, we aimed to innovate the texture-customizable composite products with specific physio-chemical and functional properties by mixing peach pectin and SPI, which could cater to the dietary needs of individuals who have difficulty in chewing or swallowing, or those who do not consume enough high-protein foods. Here, we first investigated the properties of WSP, CSP and NSP from peaches, including neutral sugar composition, nuclear magnetic resonance (NMR) spectra, and MW distribution. After that, SPI was mixed with pectin fractions to form pectin-SPI gels. Following the mixing strategy, the effect of pectin fractions on physicochemical properties and macro- & micro- structure of the pectin-SPI composite gels was investigated. Furthermore, the formation mechanism of the pectin-SPI composite gels was also studied based on the characteristics of pectin fractions. This exploration extends to enrich the textural diversity to cater to the consumer's demands for varied textures, which will broaden the application of pectin and SPI in novel composite food products.

2. Materials and methods

2.1. Materials

Peach (*Meirui*) was obtained from the Beijing Hualian supermarket (Beijing, China). SPI (protein purity ≥90 %, analytical grade) was obtained from Yuanye Bio-Technology Co. Ltd. (Shanghai, China). Bovine serum albumin (BSA) protein concentration assay kit was obtained from Yuanye Bio-Technology Co. Ltd. (Shanghai, China). All chemicals were analytical grade and obtained from Solaibao Technology Co., Ltd. (Beijing, China).

2.2. Preparation of pectin fractions

Peach pectin fractions were extracted from peach according to Wang et al. [5] with small modifications. After washing and slicing, peaches without kernels were freeze-dried. The dried peach (5.00 ± 0.10 g) was thoroughly blended with 250 mL of 70 % ethanol for 2 h using an IKA disperser (T25 digital ultra-turrax, IKA Inc., Germany). This process was repeated 3 times. Subsequently, the residue was mixed with 150 mL acetone for 5 min. Ultimately, the remaining residue, identified as alcohol insoluble residues (AIR), was produced. AIR (0.50 ± 0.01 g) was added to 90 mL of distilled water and continuously maintained at 100 °C with stirring on a magnetic stirrer (RT, IKA Inc., Germany) for 10 min. The filtrate was dialyzed against distilled water for 72 h and subsequently freeze-dried, resulting in a product designated as WSP. The residue was combined with 90 mL of 0.05 mol/L cyclohexane-trans-1,2-diamine tetra-acetic (CDTA) with 0.1 mol/L potassium acetate and stirred continuously for 6 h. The pH was set to 6.5 using 0.1 mol/L HCl. The filtrate was initially dialyzed against 0.1 mol/L NaCl for 36 h and then with distilled water for another 36 h. After freeze-drying, it was marked as CSP. The remaining residue was treated with 90 mL of 0.05 mol/L Na_2CO_3 in 0.2 mol/L $NaBH_4$ for 16 h with continuous stirring at 4 °C, then allowed to sit at room temperature for an additional 6 h. This filtrate was dialyzed against distilled water for 72 h, freeze-dried, and identified as NSP.

2.3. Neutral sugar content

Neutral sugars in pectin fractions were analyzed using an ICS-3000 Ion Exchange Chromatography system (USA), with a Carbo Pac PA20 column and a pulsed amperometric detector, following the method described by Yu et al. [16]. Pectin (5.00 ± 0.01 mg) was hydrolyzed with 2 mL 2 mol/L trifluoroacetic acid for 1 h at 110 °C. The hydrolysate was diluted and filtered through a 0.22 μm filter before injection (10 μL samples) into the chromatography system. The elution used a gradient program with (S1) Milli-Q water, (S2) 0.20 mol/L NaOH, and (S3) 1.00 mol/L NaAC as eluents at a rate of 1.0 mL/min, maintaining the column at 35 °C. The gradient program was set as follows: 0–20 min with 91 % S1 and 9 % S2; 20–20.1 min with 86 % S1, 9 % S2 and 5 % S3; 20.1–40 min: 71 % S1, 9 % S2 and 20 % S3; 40–60 min with 100 % S2; and 60–70.1 min with 91 % S1 and 9 % S2. Standards including galacturonic acid (GalA), rhamnose (Rha), fucose (Fuc), arabinose (Ara), galactose (Gal), glucose (Glc), mannose (Man) and xylose (Xyl) were employed for identification and quantification of sugars.

2.4. NMR spectra

The freeze-dried pectin (10 mg/mL) was fully dissolved into D_2O (0.50 mL) for deuterium exchange, followed by lyophilization. The isotope-exchange step was repeated three times. High-resolution ^{1}H and ^{13}C NMR spectra were obtained using a 600 MHz NMR spectrometer (Bruker Avance NEO 600, Bruker Inc., Switzerland) at 25 °C. Data was analyzed by MestRenova software (MestreLabResearch, Santiago de Compostela, Spain) [17].

2.5. MW distribution

The MW distribution of pectin was collected by high performance size exclusion chromatography (HPSEC) (Wyatt Technology, Santa Barbara, CA, USA). MW was obtained according to the method described by Zhou et al. [18]. The HPSEC system was equipped with a laser light scattering detector, an L-2400 UV detector, a TSK Gel G4000PWxl column and an Optilab rEX differential refractometer. Pectin solutions at a concentration of 1 mg/mL were eluted through the column at 35 °C using 0.1 mol/L NaCl as the mobile phase at a flow rate of 0.5 mL/min. The refractive index increment (dn/dc) was set at 0.135 mL/g and the data collection and analysis were performed using Astra software

(Version 5.3.4, Wyatt Technology) [5].

2.6. Gel preparation

In order to prepare the uniform solutions, SPI solution (10 % *w*/w) and pectin solutions, namely, WSP, CSP and NSP (2 % w/w) were stirred using magnetic stirrers (500 rpm) at 25 °C for 2 h, respectively. SPI and pectin solutions were combined in a ratio of 9:1 (*w*/w) and stirred at 500 rpm/min on a magnetic stirrer for 1 h, followed by heating at 90 °C for 30 min and cooling in ice water bath to form the gels. The composite gels prepared by the WSP, CSP and NSP were labeled as WSP-SPI, CSP-SPI and NSP-SPI respectively.

2.7. Turbidity

Turbidity was analyzed by a UV spectrophotometer (UV-1800, Shimadzu, Japan) with the wavelength of 400 nm to achieve 100 % transmittance (T). Turbidity was expressed as 1 – T [19]. Gel samples were firstly diluted 10 times with Milli-Q water and then tested at 25 °C. Each sample was detected in 3 measurements at 1 min intervals.

2.8. Particle size

Particle size distribution was measured with a laser particle size analyzer (S3500, Microtrac, USA) with an aligned detector and laser. Before testing, gel samples were diluted 10 times with Milli-Q water. Each sample underwent three measurements, with 15 runs per measurement, and each run extended for a duration of 10 s after calibrating the backgrounds. D [3,4] was the volume mean diameter to evaluate big particles as well as D [2,3] was the area mean diameter to assess small particles. D50 was performed as the median diameter, referring to the particle size corresponding to the cumulative frequency of 50 % [20].

2.9. Rheological properties

The rheological properties of gels were measured by a rheometer (Physica MCR301, Anton Paar, Austria) with a parallel plate geometry (40 mm) and a 1 mm measuring gap in frequency sweep [11]. Flow curves for the samples were constructed using a continuous shear rate from 0.01 s^{-1} to 100 s^{-1} at 25 °C. The storage modulus (G′) and loss modulus (G″) were measured with angular frequency from 0.1 rad/s to 100 rad/s and a fixed strain of 0.5 % at 25 °C. In order to ensure that the structures of samples would not be destroyed from stress or applied strain, the 0.5 % strain was selected in all samples with their linear viscoelastic region.

2.10. Low field nuclear magnetic resonance (LF-NMR)

The moisture status of the gels was assessed using the transverse relaxation time (T_2) through an LF-NMR analyzer (MiniMR-60, Niumag Analytical Inc., Suzhou, China), which features a 0.5 T permanent magnet producing a proton resonance frequency of 23.2 MHz at 32.00 °C. Measurement parameters for T_2 relaxation included a waiting time (TW) of 2000 ms, an echo time (TE) of 0.5 ms, 12,000 echoes (NECH), and 4 scans (NS). The raw data were analyzed using logarithmic coordinates to construct T_2 distribution curves with a multi-exponential model, facilitated by the MultiExp Inv Analysis software (Niumag Analytical Inc., Suzhou, China) [21].

2.11. Fourier transform infrared spectroscopy (FT-IR)

Freeze-dried samples were mixed with KBr powder (1:100, *w*/w) to prepare the pellet to obtain FT-IR spectra at room temperature. The FT-IR spectrophotometer (Tensor 27, Bruker, Germany) was configured with a resolution of 4 cm^{-1}, 64 cumulative scans, and a wavelength range from 4000 cm^{-1} to 400 cm^{-1} [11].

2.12. X-ray diffraction (XRD)

Freeze-dried samples were obtained by an XRD detector (D8 advance, Bruker, Germany). Pectin from peaches, freeze-dried gels and SPI were analyzed using coKα radiation (λ = 1.7889 Å). The XRD detector scanning was conducted over a 2θ range from 5 to 55° at a rate of 2°/min^{-1}. The XRD detector worked with 40 kV and 30 mA conditions.

2.13. Microstructure

The microstructure of freeze-dried samples was measured using scanning electron microscopy (SEM) (Gemini 300, ZEISS, Germany) and the surface morphology of the samples was measured using an energy dispersive X-ray spectroscopy (EDX) (Smartedx, ZEISS, Germany). The magnification was of 50×. The acceleration voltages were 3 kV for SEM and 15 kV for SEM-EDX, respectively [23].

2.14. Chemical forces of gels

The chemical forces of the gels were determined by the method of Shi et al. [24] with small modifications. Gels (0.10 ± 0.02 g) were mixed with 5.00 mL of each denaturing solution for 30 min, followed by centrifugation at 5000 ×*g* for 10 min at 25 °C. Details of solution preparation were shown in Table 1. Controls and blanks were prepared for all denaturing solutions to account for background interference, and a dialysis was performed before measurement to remove β-mercaptoethanol interference. The results were determined based on the protein content in the denatured solutions, which was estimated using a BSA protein concentration assay kit. Ionic bonding was quantified by the difference in protein solubility between S2 and S1, hydrogen bonding between S3 and S2, hydrophobic interactions between S4 and S3, and disulfide bonding between S5 and S4.

2.15. Molecular docking

The molecular docking was performed by Autodock vina software (version 1.1.2, Molecular Graphics Lab of Scripps Research Institute, USA), and the structure diagram was drawn by PyMol software (Version 2.5, Schrödinger, LLC.). Based on the macromolecules' properties, galacturonan (galacturonic acid, CID 5459352) from PubChem was selected as the pectin model. The protein structure of 11S (glycinin, PDB ID: 1FXZ) and 7S (β-conglycinin, PDB ID:1IPK) were obtained from the Uniprot data bank [25].

2.16. Statistical analysis

All experiments were performed in triplicate. Data were analyzed by Tukey's test for statistical relevance and one-way analysis of variance for significance at $p < 0.05$, which was performed by utilizing SPSS.19.0 software (IBM Crop., Armonk NY USA). Origin 9.0 software (Origin Lab, Northampton, USA) and PowerPoint (Version 2019, Microsoft Inc., Washington, USA) were used to graph the results.

Table 1
Composition of different denaturing solutions.

	Solution formulation
S1	Sodium chloride solution (0.05 mol/L)
S2	Sodium chloride solution (0.6 mol/L)
S3	Sodium chloride solution (0.6 mol/L) + urea solution (1.5 mol/L)
S4	Sodium chloride solution (0.6 mol/L) + urea solution (8.0 mol/L)
S5	β-Mercaptoethanol (0.5 mol/L) + sodium chloride solution (0.6 mol/L) + urea (8.0 mol/L)

3. Results and discussion

3.1. Structural characteristics of pectin fractions

3.1.1. DM and neutral sugar content

As depicted in Table 2, the DM of WSP was 66.15 %, indicating that WSP was HMP. While CPS with a low DM value (32.01 %) was LMP. Additionally, no DM value was shown in NSP because of the demethylation during extraction.

Neutral sugars were marked as the structural fingerprint of pectin. GalA was the dominant monosaccharide in WSP, CSP and NSP, illustrating that HG region, consisting of the repeated GalA units, predominated in pectin structure. Especially, for WSP, Gal, Ara and Rha were the main neutral sugars in pectin backbone, demonstrating the abundant RG-I region in WSP. This result was also described in yellow peach by Wang et al. [5]. Considering the high contents of Glc and Xyl, WSP was also rich in neutral sugar side chains of the RG-II region. As for CSP, neutral sugars with low content suggested the small side chain. NSP enriched in Ara and Gal highlighted the plentiful side chains, probably resulting from the RG-I region [3]. NSP was also enriched in the RG-II region, because of the highest value of Fuc (0.29 mg/g AIR), which was a composition from the RG-II region [4].

Sugar ratios offer insight into structural configuration of pectin. Sugar ratio A, defined as GalA / (Fuc + Rha + Ara + Gal + Xyl), elucidates the linearity of pectin molecules. CSP with the highest sugar ratio A was characterized by the highest linearity, followed by WSP and NSP fraction. Sugar ratio B, defined as (Ara + Gal) / Rha, provides an estimation of the branching degree of the RG-I region. As seen particularly in WSP and NSP, high values in sugar ratio B, were indicative of a highly branched structure [18]. CSP with the lowest sugar ratio B depicted the poor RG-I region. Simply, WSP and NSP were rich in RG-I and RG-II regions, while CSP had a higher linearity.

3.1.2. MW distribution

MW is a measure that describes the sum of the atomic weight values. It could be observed that weight-average molecular weight (Mw) and number-average molecular weight (Mn) were significantly varied from the pectin fractions (Fig. 1a and Table 2). CSP showed the lowest Mw with the value of 5.59×10^4 g/mol, while WSP possessed the highest Mw (7.50×10^4 g/mol). For Mn values, CSP > WSP > NSP. The lowest Mw/Mn value, namely polydispersity, was found in CSP, indicating the narrowest MW distribution. Considering the highest Mw/Mn ratio (7.11), NSP exhibited the greatest polydispersity, suggesting a broad spectrum of molecular sizes. In addition, WSP had a broad MW distribution (10.54–19.35 min) with a higher peak (Fig. 1a), indicating a wide range in molecular weights and that the main components had larger molecular weights. CSP exhibited a lower peak (10.56–18.99 min), slightly later than WSP, which might suggest that the average MW of CSP was smaller than that of WSP. Unlike WSP and CSP, NSP exhibited two peaks, suggesting more polydisperse than WSP and CSP. The elution profile of NSP was concentrated in the lower molecular weight area, indicating that its molecular weights are generally smaller.

3.1.3. NMR spectra

The baseline of NMR spectra was stable, only with little noise, indicating excellent purity and concentration of the sample, as well as proper instrument calibration. Generally, the varied intensities of the peaks with pronounced signals usually indicate a high concentration or more protons in samples [26]. Furthermore, the overlap of signals always demonstrated similar types of protons, however, differences in intensities and chemical shifts performed the distinct structural properties among samples [17]. ^{1}H NMR spectra of samples were shown in Fig. 1b. The maximum signal was found at 3.69/3.59 ppm in WSP/CSP, aligned with the signal peak of -OCH_3 of esterified galacturonic acid [27]. As demethylation took place during NSP extraction, only a diminished methoxy signal was detected. Five major signals, namely

Table 2
DM, neutral sugar content and molecular weight of pectin fractions.

	DM (%)	Manosaccharide (mg/g AIR)								Sugar ratio		Mn (g/mol)	Mw (g/mol)	Mw/Mn
		GalA	Fuc	Rha	Ara	Gal	Glc	Xyl	Man	A	B			
WSP	66.15 ± 0.40	72.38 ± 2.63c	0.14 ± 0.04b	2.11 ± 0.16b	2.88 ± 0.03a	3.65 ± 0.10c	1.51 ± 0.80c	1.22 ± 0.10c	0.38 ± 0.03b	7.24 ± 0.55c	3.10 ± 0.17b	7.50E+04	2.51E+05	4.28
CSP	32.01 ± 0.04	45.60 ± 2.69a	0.07 ± 0.02a	1.69 ± 0.06a	2.72 ± 0.06a	0.93 ± 0.05a	0.57 ± 0.04a	0.22 ± 0.05a	0.06 ± 0.02a	8.09 ± 0.44b	2.15 ± 0.17a	5.59E+04	2.46E+05	3.28
NSP	–	52.19 ± 2.23b	0.29 ± 0.04c	1.79 ± 0.29ab	2.81 ± 0.22a	3.18 ± 0.14b	1.24 ± 0.14b	0.41 ± 0.06b	0.48 ± 0.09b	6.14 ± 0.20a	3.42 ± 0.62b	6.40E+04	4.54E+05	7.11

Note: Values were expressed as averages ± standard deviations. Values followed by the different lowercase letters in the same column had significantly differences ($p < 0.05$). DM: degree of methoxylation; Mw: weight-average molecular weight; Mn: number-average molecular weight; WSP, water-soluble pectin; CSP, chelator-soluble pectin; NSP, Na_2CO_3-soluble pectin. GalA: galacturonic acid; Fuc: fucose; Rha: rhamnose; Ara: arabinose; Gal: galactose; Glc glucose; Man: mannose; Xyl: xylose.

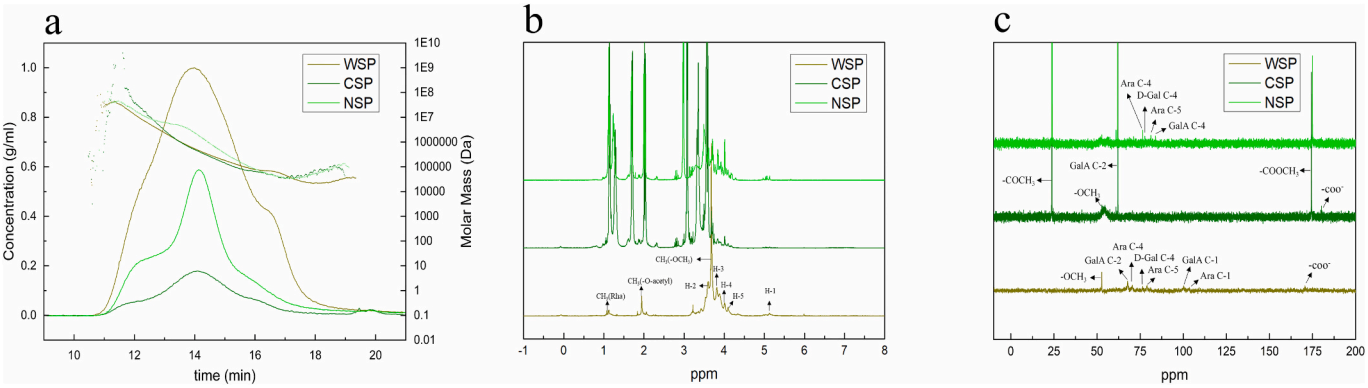

Fig. 1. Structural characteristics of three pectin fractions, Molecular weight (a), NMR spectra of ^{1}H (b) and ^{13}C (c).
Note: Concentration is represented by a solid line, and Molar Mass is represented by a dashed line in Fig. 1a.

5.13/5.05/5.06, 3.61/3.37/3.50, 3.82/3.69/3.67, 4.01/4.01/4.02, 4.10/4.10/4.09 ppm, corresponding to H-1 to H-5 in WSP/CSP/NSP, respectively, were attributed to protons of esterified GalA units. These results also confirmed that GalA was dominant in pectin fractions [26]. The galacturonic acid backbone of pectin linked by →4)-α-GalA-(1 → was also elucidated by these five major signals. Peaks at 1.09, 1.20 and 1.19 ppm for WSP, CSP and NSP, respectively, corresponded to →2)-α-Rhap-(1→, which verified RG-I region was prominent in the structure of pectin fractions [17,28]. Additionally, NSP showed a stronger signal around 5.1 ppm, corresponding to Ara, than WSP and CSP due to high RG-I region [17]. The characteristic proton peaks around 2.0 ppm were corresponded to acetyl groups, confirming the presence of acetylation in CSP and NSP [28].

^{13}C NMR spectra were depicted in Fig. 1c. For WSP, signals at 52.86 and 170.87 ppm were assigned to -OCH_3 and -COO^{-}, respectively [28]. Peaks at 67.86, 76.63 and 100.08 were derived from GalA C-2, D-Gal C-4 and GalA C-1, respectively [17]. The chemical signals at 70.56, 78.98 and 103.11 were derived from Ara C-4, Ara C-5 and Ara C-1 [27], which also confirmed the highest Ara content in WSP. Together with neutral sugar analysis and NMR spectra, it was reasonable to conclude that the RG-I region was the dominant one for WSP. Differing from WSP and NSP, CSP only showed a few characterized peaks. In detail, the chemical shift in CSP at 53.95 and 62.09 ppm were assigned to -OCH_3 and GalA C-2, respectively [17]. The peak observed at 23.93 ppm was contributed to the acetyl methyl carbon of CSP. For NSP, the domain chemical shift was observed at 61.93 ppm, corresponding to GalA C-2. The peaks at 76.45, 78.30, 81.21 and 83.84 were derived from Ara C-3, D-Gal C-4, Ara C-5 and GalA C-4, respectively [17,27]. The acetyl methyl carbon peak in NSP was identified at 23.89 ppm [29]. The NMR spectra analysis further identified the plenty of side chains in NSP, which was associated with the analysis of neutral sugar. In addition, significant peaks related to -OCH_3 and -COO^{-} were obtained in WSP and CSP, but not in NSP. By combining the analysis of NMR and monosaccharide composition, it could be determined that WSP, CSP and NSP were primarily composed of a → 4)-α-GalA-(1 → linked galacturonic acid backbone HG. Additionally, the RG-I region, which was formed by the attachment of neutral sugars Gal, Glc, and Ara to some of the chains, was also exhibited in the three pectins. Specifically, WSP and NSP displayed more RG-I region.

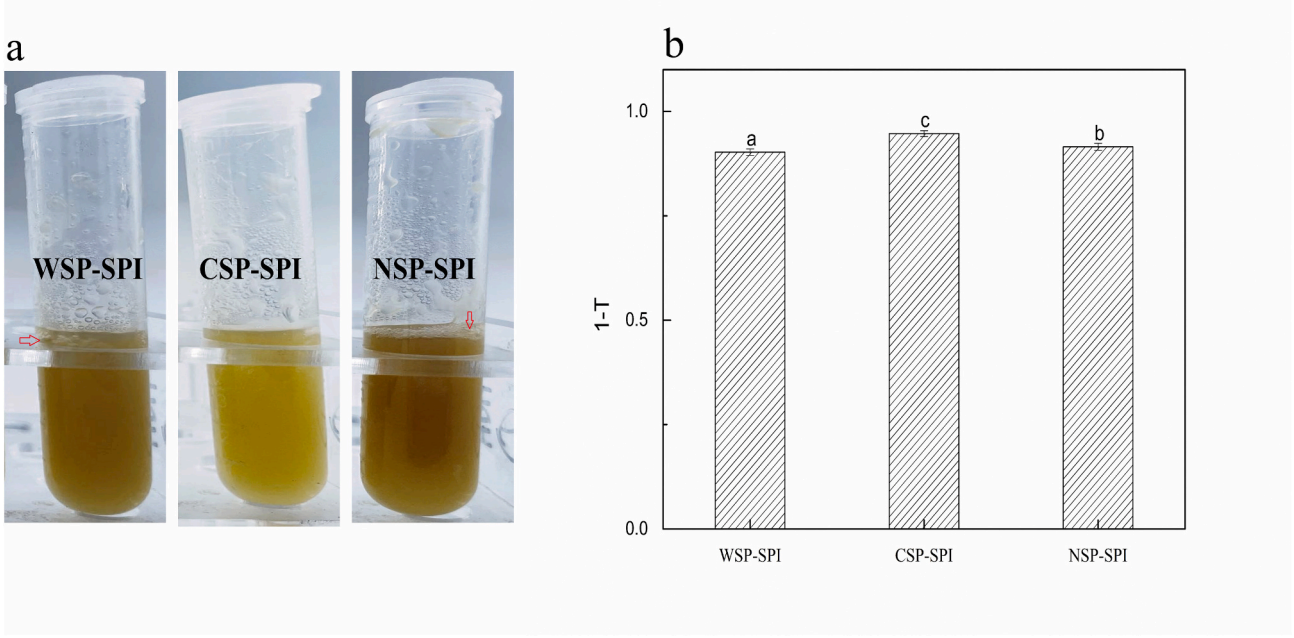

Fig. 2. Appearance (a) and turbidity (b) of pectin-SPI gels.
Note: Different lowercase letters indicate significant differences among treatments ($p < 0.05$).

3.2. Morphological and structural characteristics of pectin-SPI gels

3.2.1. Appearance and turbidity

When subjected to SPI, all pectin fractions formed gels, however, significant differences in appearance among pectin-SPI gels were obtained (Fig. 2a). Slightly liquid separation at the top was observed in WSP-SPI and NSP-SPI gels, indicating phase separations had occurred in the system. This resulted in multiphase structures, demonstrating poor compatibility. Meanwhile, CSP-SPI gel kept a stable state without any layering, suggesting that CSP and SPI exhibited good compatibility in this system, forming a single-phase mixture.

The turbidity of pectin-SPI gels was depicted in Fig. 2b. Turbidity is usually used to describe the cloudiness or haziness of insoluble composites, which is driven by electrostatic attractions between oppositely charged molecules [30]. CSP-SPI showed the highest turbidity (0.95), indicating the lowest transmittance as well as the increased scattering of light [19]. The highest turbidity could be attributed to the strong unfolding of SPI and the formation of pectin-SPI aggregation during the heat treatment [14]. CSP carried with abundant binding sites for hydrophobic interactions, contributing to the high binding ability, resulting in more pectin-SPI aggregation. Such a result was also observed in the case of sugar beet pectin and pea protein gel [31]. The high turbidity in CSP-SPI made it suitable for industry products in which cloudiness and density were desired. WSP-SPI had the lowest turbidity (0.90), suggesting weak formation of insoluble composites since high MW of WSP, alongside fine solubility and dispersion of particles, which inhibited aggregation. This was preferred for clear solutions applications, such as beverages [14].

3.2.2. FT-IR

FT-IR was employed to perform the chemical bond stretching and conformational changes in pectin structures (Fig. 3). For all samples, a wide and strong absorption peak was observed in the range from 3000 cm^{-1} to 3700 cm^{-1} corresponding to O—H stretching vibration [32]. As for SPI, three characteristic peaks, namely around 1590–1710 cm^{-1}, 1490–1590 cm^{-1}, and 1240 cm^{-1}, were obtained from amide I, amide II, and amide III, respectively. The featured peaks at 1656 cm^{-1} and 1530 cm^{-1} in SPI were related to the C═O stretching in amide I and N—H vibrations in amide II, respectively, while the band around 1390 cm^{-1} was reported to N—H vibrations and C—N stretching in amide III [28]. Concerning pectin fractions, the characteristic peak at 2933 cm^{-1} was corresponded to C—H vibrations. Absorption bands around 1740 cm^{-1} and 1620 cm^{-1} were related to methyl esterified carbonyl group and the ionic carboxyl group, respectively, which were both related to DM of pectin [16]. The differences in these two peaks between WSP and CSP suggested the distinct DM values, which were in accordance with UV detector-DM values results (Table 2). The peak between 2950 cm^{-1} and 2850 cm^{-1} arose from the stretching of methyl esters groups (O-CH_3) of galacturonic acid [16]. The characteristic peaks between 800 and 1200 cm^{-1} were associated with the fingerprint area of pectin, suggesting that pectins were rich in uronic acid. In particular, several small absorption bands were obtained in 1400–1200 cm^{-1}, referred to C-O-H bend deformation and C—O stretch vibration [5]. The intensities of absorption bands in 1400–1200 cm^{-1} varied significantly from different pectin fractions, which were also supported by NMR results. In terms of pectin-SPI gels, the O—H absorption bands (3396–3294 cm^{-1}) were wider and shifted towards lower wavelengths compared to O—H absorption band in SPI (3460 cm^{-1}), suggesting the strengthened hydrogen bonds as pectin incorporation [32].

After compounding with SPI, the spectra of pectin-SPI gels were nearly identical, revealing that SPI incorporation introduced additional functional groups. Compared with pectins, the spectra in the range of 1400–1200 cm^{-1} for pectin-SPI gels were smoother, suggesting the new formation of aggregation. Following pectin addition, the absorption bands of amide I (1590–1710 cm^{-1}) and amide II (1490–1590 cm^{-1}) moved to a lower wavelength indicating the more regular network structure was formed in pectin-SPI gels [32]. Compared to SPI, the characteristic peak (1530 cm^{-1}) in pectin-SPI gels, attributed to -NH_2 groups, was sharply decreased illustrating that -NH_2 groups participated in the aggregation accompanied by a new substance born. Additionally, the newborn bands of C═N stretching vibration (around 1658 cm^{-1}) in pectin-SPI spectra also identified the new aggregation formation.

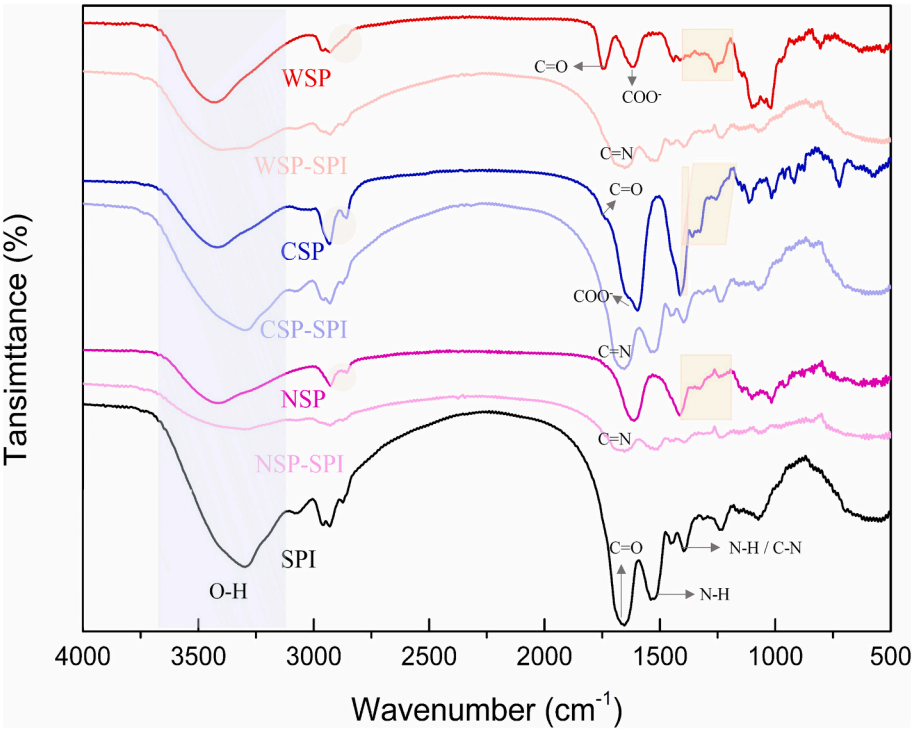

Fig. 3. FT-IR spectra of SPI, three pectin fractions and pectin-SPI gels.

Especially for CSP-SPI, we observed the widest band of C═N, which depicted the strongest interaction [28].

Results showed a significant relationship between the protein's secondary structure and amide I band. Therefore, FT-IR spectral analysis from 1700 to 1600 cm^{-1} was conducted to assess the secondary structure of the protein (including α-helix, β-sheet, β-turn, and random coil) [13]. For the secondary structure of SPI, β-sheet was predominant, followed by β-turn (Table 3). Following SPI addition, β-sheet and β-turn were significantly increased, while α-helix and random coils were pronouncedly decreased in gels, implying an enhanced regular structure in gels as well as a steady network. This phenomenon might result from the increased charge and intermolecular repulsion within gels, which facilitated the readily bound between intermolecular protein chains [33]. Generally, the hydrophilic environment did not benefit for the formation of hydrogen bonds between water molecules and proteins, associated with the reduced content of α-helix. As the formed hydrogen bonds among neighboring spirals decreased during the compounding procedure, the elongation of protein chains and adoption of U-shaped folding of protein was enhanced, which also promoted the structure transition from α-helix to β-sheet and β-turn [34]. Furthermore, β-sheet formation was attributed to a regular hydrogen bond forming between carbonyl oxygen (-C═O) and amide hydrogen (-CONH-) of the same or adjacent protein chain [33]. Specifically, compared with SPI, WSP-SPI showed a decrease in α-helix by 38.92 % and a decrease in random coils by 0.49 %. As α-helix and β-sheet were buried within the polypeptide chains, the reduction in this structure could suggest the changes in the spatial conformation of SPI accompanied by more unfolding protein when mixed with WSP. Moreover, the CSP treated strategy significantly increased the ratio of β-sheet and β-turn in CSP-SPI, which rose by 13.45 % and 7.73 %, compared to SPI, respectively. Meanwhile, α-helix in CSP-SPI was lost by 34.13 %. It should be noted that β-sheet content in CSP-SPI was higher than that in WSP-SPI. This could be attributed to CSP as the LMP brought plentiful charges into the gel and assisted the action of intermolecular repulsion, which accelerated protein unfolding and resulted in the formation of more U-shaped folds [34]. The loss of α-helix and β-turn but the increase of β-sheet was observed in NSP-SPI after the addition of SPI, which could be explained by the alteration of SPI's spatial conformation due to NSP's hydrophobic structure. The rearrangement of SPI and NSP in their spatial structure changed the original structure, and this reorganization affected the physicochemical properties of the new compound [13,28]. Regarding structure changes during the gel formation strategy, pectin fractions with multi-branched backbone boosted the covalent bonding and electrostatic interaction with SPI molecules, which stabilized the spatial structure of the pectin-SPI gels.

3.2.3. Particle size

Particle sizes of SPI and pectin-SPI gel were shown in Fig. 4a-4b. The unimodal distribution in all samples demonstrated the homogeneous aggregates size. When SPI was applied to pectin fractions, the particle size distribution peaks significantly shifted left, indicating the reduced particle size. The decreased particle sizes could be ascribed to the retarded self-aggregation of SPI molecules under the environment with high net charges and strong electrostatic repulsion caused by biopolymer clusters [35]. The shifts varied from the pectin fractions, elucidated the distinct intensities of interactions between pectin fractions and SPI. The broadest distribution in WSP-SPI suggested less homogeneity in particle size, owing to the weak intermolecular forces within the WSP-SPI system. The multi-branched WSP with large molecular weight resulted in the broadest particle size distribution of WSP-SPI, with a median particle size of 256.30 μm. The high methylation degree of WSP (DE = 66.15 %) weakened hydrophobic interactions within the SPI-WSP and SPI-SPI composite systems, potentially leading to increased particle size and flocculation [36]. Meanwhile, both CSP-SPI and NSP-SPI were characterized by sharp and focused peaks, indicating uniform particle distribution alongside strong intermolecular forces. Additionally, because of the high linearity of CSP with numerous carboxyl groups, the strong intermolecular interactions readily happened [37], resulting in smaller D [3,4], D [2,3] and D50.

Table 3
Secondary structure of SPI and pectin-SPI gels.

	β-Sheet (%)	β-Turn (%)	Random coil (%)	α-Helices (%)
SPI	39.44 ± 0.14a	23.33 ± 0.25a	20.47 ± 0.34bc	16.75 ± 0.26c
WSP-SPI	43.98 ± 0.08b	25.50 ± 0.16b	20.32 ± 0.72bc	10.20 ± 0.15a
CSP-SPI	44.72 ± 0.22c	25.13 ± 0.42b	19.08 ± 0.94ab	11.07 ± 0.48a
NSP-SPI	44.02 ± 0.17b	23.34 ± 0.38a	18.31 ± 0.50a	14.33 ± 0.52b

Note: Values were expressed as averages ± standard deviations. Values followed by the different lowercase letters in the same column had significantly differences ($p < 0.05$). SPI, soy protein isolate; WSP, water-soluble pectin; CSP, chelator-soluble pectin; NSP, Na_2CO_3-soluble pectin.

3.3. Rheological properties

The apparent viscosity of SPI and pectin-SPI gels was shown in Fig. 5a. As the shear rate increased, the apparent viscosities of all samples were firstly increased and then decreased, indicating the pseudoplastic fluids properties with shear-thinning flow behavior. The highest viscosity was found in NSP-SPI, followed by CSP-SPI and WSP-SPI, which were all higher than SPI. This enhanced apparent viscosity induced by the SPI addition strategy could be explained by the tight aggregation formation between SPI and pectin through electrostatic attraction [38], which was in line with the analysis of particle sizes. In particular, the abundant RG regions in NSP might be the predominant reason for the biggest apparent viscosity of NSP-SPI. As LMP, CSP with numerous exposed free carboxyl groups could readily entangle with SPI via strong electrostatic interaction, leading to the increased gel viscosity [37]. However, the lower apparent viscosity in WSP-SPI also suggested the small number of the WSP-SPI composite, which was also consistent with the turbidity.

The viscoelastic modulus of SPI and pectin-SPI gels was shown in Fig. 5b. Variations in storage modulus (G′) and loss modulus (G″) across angular frequencies were assigned to elastic behavior and viscous behaviors, respectively. Among all the samples, G′ was consistently higher than G″ over a wide range from 0.1 rad/s to 100 rad/s, suggesting the elastic-dominated structure of all samples [39]. Following SPI addition, the values of viscoelastic modulus pronouncedly increased, probably due to the strong hydrogen bonding within pectin-SPI gels. This result was in agreement with the whey protein isolate (WPI)-Mesona chinensis (MC) polysaccharide gel with strong rheological properties [40], in which hydrogen bonding played a crucial role [40]. As angular frequency increased, G′ and G″ were remarkably increased, suggesting the strong electrostatic attraction between pectin and SPI molecules. For SPI and NSP-SPI gels, as the angular frequency increased (up to 100 rad/s), the G′ value produced an intersection with the G″ value (G′ = G″), illustrating a weak gel behavior was formed within under high shear force. Meanwhile, the G′ values in WSP-SPI and CSP-SPI gels were always greater than G″ within the range of 0.1–100 rad/s, highlighting the gel behavior. CSP-SPI demonstrated the highest G′ and G″, contributing to the high linearity, less neutral sugar side chains of CSP, which was preferred to exposure enough binding sites to bind with SPI [31]. However, the abundant RG-I region in NSP could explain the poor viscoelastic modulus of NSP-SPI.

3.4. LF-NMR

LF-NMR utilized relaxation times to assess moisture content and movement within SPI and pectin-SPI gels (Fig. 6). Specifically, the transverse relaxation time, denoted as T_2, was particularly sensitive to identifying distinct forms of water and characterizing the mobility of water types. A reduced T_2 value indicated a closer association between

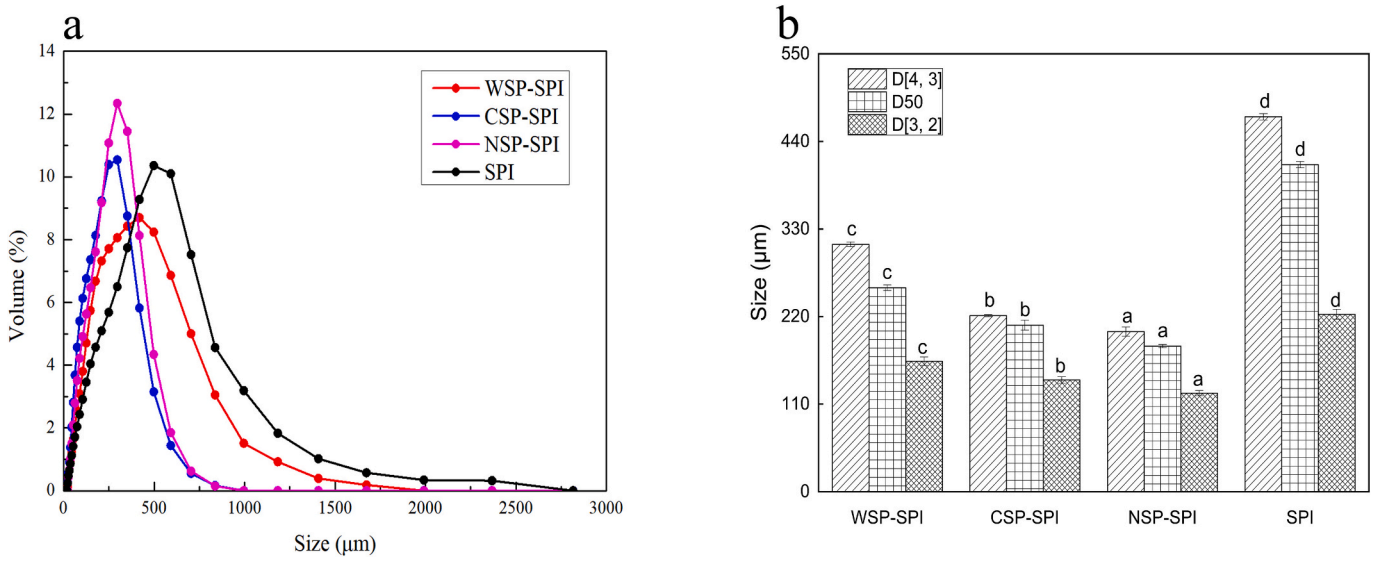

Fig. 4. Particle size distribution (a) and D [3,4], D50 and D [2,3] (b) of SPI and pectin-SPI gels.
Note: Different lowercase letters indicate significant differences among treatments ($p < 0.05$).

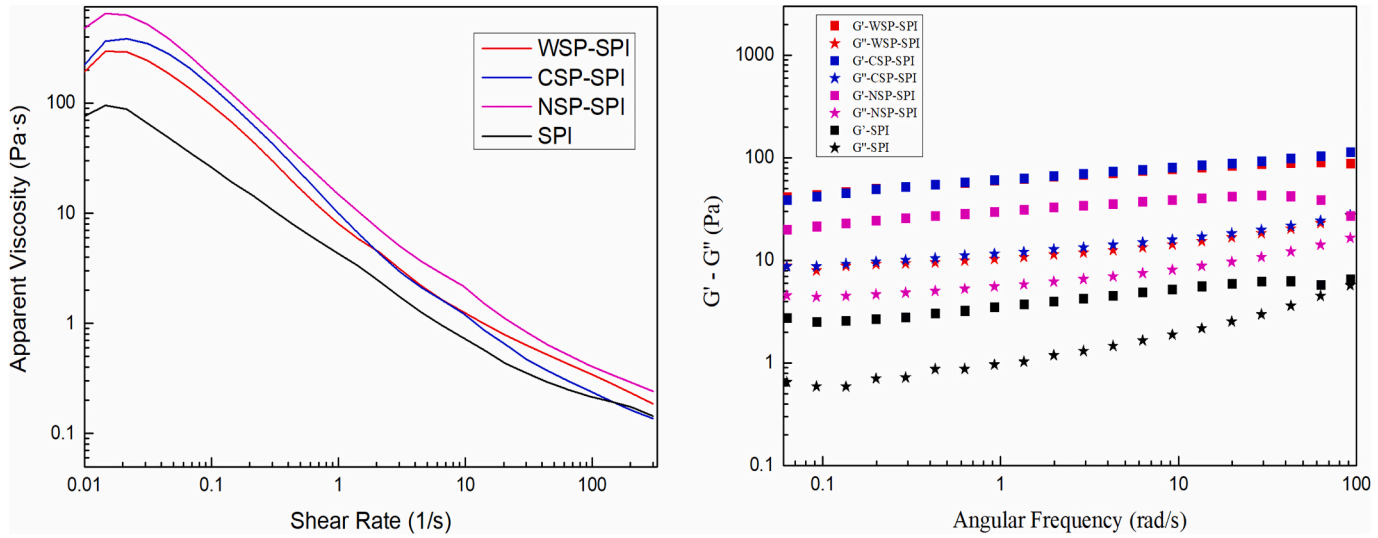

Fig. 5. The rheological properties of SPI and pectin-SPI gels, apparent viscosity (a), storage modulus (G′) and loss modulus (G″) (b).

water and gel matrix, as well as pronounced interactions between water molecules and macromolecules [41]. Three prominent peaks of water distribution were observed, namely, 0.56–2.24 ms (T_{2b}), 5.17–13.67 ms (T_{21}), and 117.58–471.37 ms (T_{22}), respectively. Specifically, T_{2b} is correlated with water which exhibits the most intense interactions within the macromolecules. T_{21} corresponds to water confined within the gel network structure. T_{22} is indicative of water that is immobilized within the network of gel [42]. Immobilized water was dominant in all samples. With the incorporation of pectin, T_2 was significantly left-shifted, indicating a strong water-binding capacity in the gels. Furthermore, the post-heating processing might also accelerate protein unfolding and increase the exposure of hydrophobic groups, which facilitated the formation of salt bridges between protein and metal ions (e.g. Ca^{2+}, naturally present in the pectin-protein composites) [34,43]. This behavior was preferred to capture water and reduce its mobility [44]. T_{2b} in pectin-SPI gels were all pronounced left-shifted in comparison with SPI, indicating the reduced water mobility owning to the strengthened strong hydrogen bonds within the composite system [41]. WSP-SPI and NSP-SPI depicted shorter T_{2b} than CSP-SPI, which might be attributed to the development of the network structure formed by abundant side chains brought by WSP and NSP that held water in a less mobilized state. The shortest T_{21} was demonstrated in CSP-SPI, indicating the tightly locked water in a dense network. In this situation, CSP, as LMP with numerous carboxylates, could effectively affect the microstructure, thereby contributed to the improved water capture. Taken together, the reduced water mobility suggested the strong water holding capacity of the pectin-SPI composite gels, which might contribute to the increased stability of the composites matrix.

3.5. XRD

Further supporting these structural insights, XRD tests were applied to perform the characteristic peaks of crystallization structure from pectin fractions, SPI and pectin-SPI gels (Fig. 7). The XRD pattern of SPI displayed two characteristic peaks ($2\theta = 8.82°$ and 19.90°) with the wide ranges, indicating the partially crystalline state. In contrast, two intense peaks ($2\theta = 16.03°$ and 22.32°) were detected in WSP. While three intense peaks were observed at CSP and NSP. Specifically, the

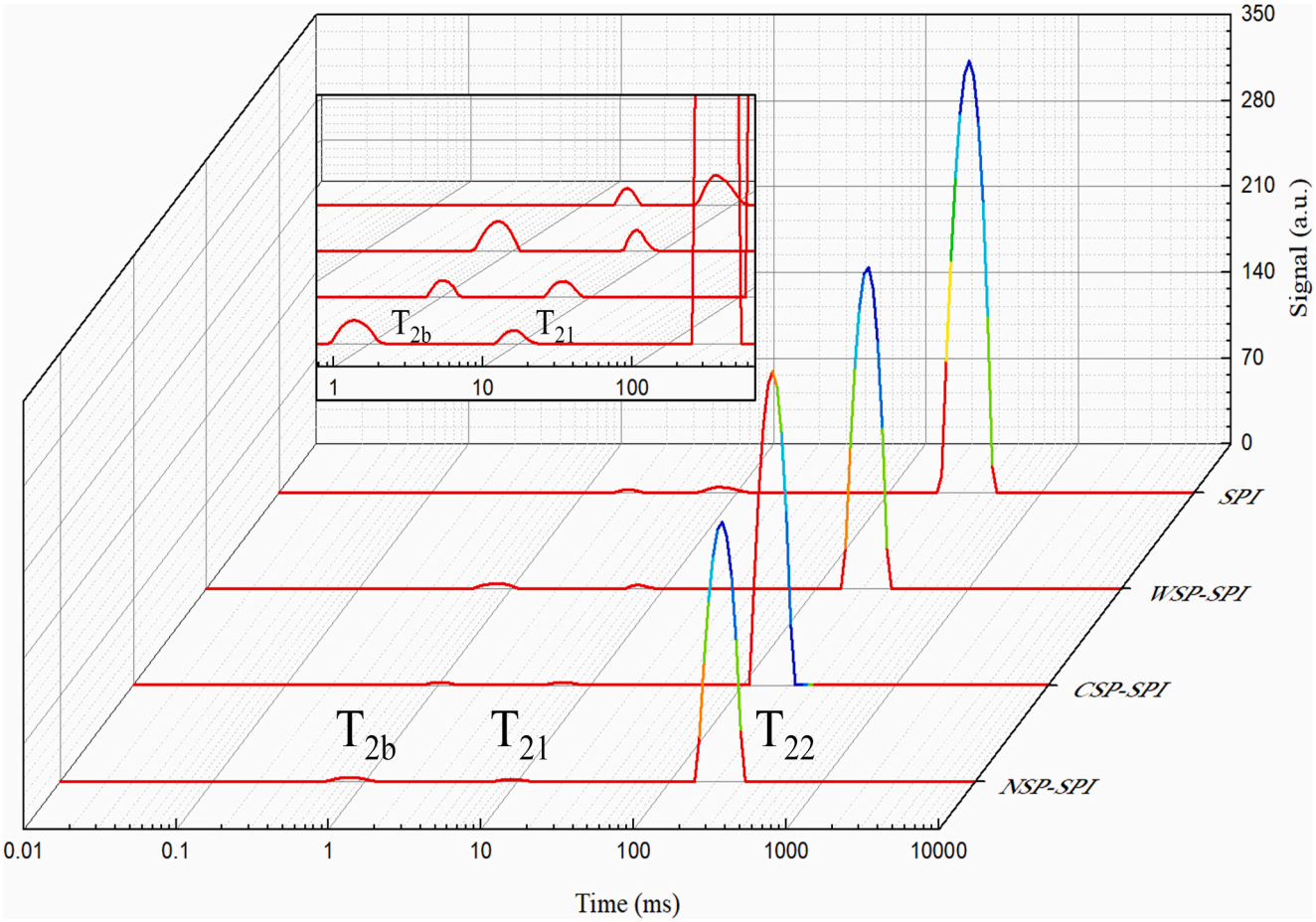

Fig. 6. The transverse relaxation (T_2) curves of SPI and pectin-SPI gels.

peaks occurred at 8.37° and 5.2°, 15.29° and 15.98°, and finally at 22.34° and 22.38°, respectively. These results implied that the pectin fraction could be considered as the crystalline material. When subjected to SPI compounding, the peak around 15°-16° disappeared, indicating the formation of new gels. Compared with SPI, the diffraction angles of pectin-SPI gels shifted to shorter 2θ, which also suggested the formation of hypocrystalline composites. This was consistent with results of MC polysaccharide-WPI gels [42]. As for pectin-SPI gels, CSP-SPI showed a sharp diffraction peak and high diffraction intensity, suggesting increased crystallinity [19]. Meanwhile, the low and broad peaks were obtained in WSP-SPI, indicating a low crystalline structure. Early research believed the characteristic diffraction peaks of pectin became gradually broader and more diffused as DE increased [17], which supported the result of the WSP-SPI gel in our study. Briefly, the addition of SPI in the pectin fractions could improve the conformational state and intermolecular interaction, which benefited the network structure and the viscoelastic performance of gels. Above all, XRD analysis revealed the formation of new complexes between pectin and SPI, as indicated by FTIR.

3.6. SEM and SEM-EDX of pectin-SPI gels

Fig. 8a provided visual evidence of the effect of pectin fractions on microstructure of pectin-SPI gels. The non-homogeneous SPI particles were observed with smooth areas and folded regions. WSP-SPI showed a relatively smooth and homogenous structure with few porosities, indicating the uniform distribution of WSP and SPI molecules in the gel. This also suggested good compatibility between WSP and SPI, which resulted in a homogenous structure. As the increased binding of carboxyl groups of CSP to SPI, the CSP-SPI displayed a dense and composite network with regular layer adjacence, which could explain its good stability. Additionally, the CSP-SPI network structure with large pore size and dense micro-network structure confirmed the great crosslinking between CSP and SPI [45]. The morphological observations depicted the strong water holding capacity of CSP-SPI, which was also corroborated by the LF-NMR analysis. Additionally, an irregular porous network but with smooth areas was observed in NSP-SPI. NSP with abundant RG regions and the greatest polydispersity might flexibly interact with SPI through various chemical groups, which might be responsible for the amorphous pore structure [26]. In summary, the pectin addition strategy promoted the formation of the dense and uniform structure within pectin-SPI matrix, which might relate to the improved rheological properties (e.g, the increased viscosity and G' and G") as well as the improved water holding capacity.

Furthermore, the element percentage and mapping in samples were depicted in Table 4 and Fig. 8b, respectively. All elements were uniformly distributed in the SPI smooth region. Compared with SPI, the element mapping of pectin-SPI gels was varied from the three pectin fractions. Elements were non-uniform distribution in mapping. The backbone structure of the gel was composed of C, O and N. C and O were the main components of pectin, suggesting the high interaction of SPI and pectin in the gels. Proper dispersion of P in pectin-SPI was obvious. Pectin induced the aggregation of Ca towards the backbone of pectin-SPI gels, especially in CSP-SPI and NSP-SPI. In CSP-SPI and NSP-SPI, the enrichment of S at the skeletal structure implied that SPI was highly attracted to CSP and NSP [46]. CSP had the highest concentration of S (0.55 %), Ca (0.15), and P (0.63), confirming LMP was easy to bind with Ca [47].

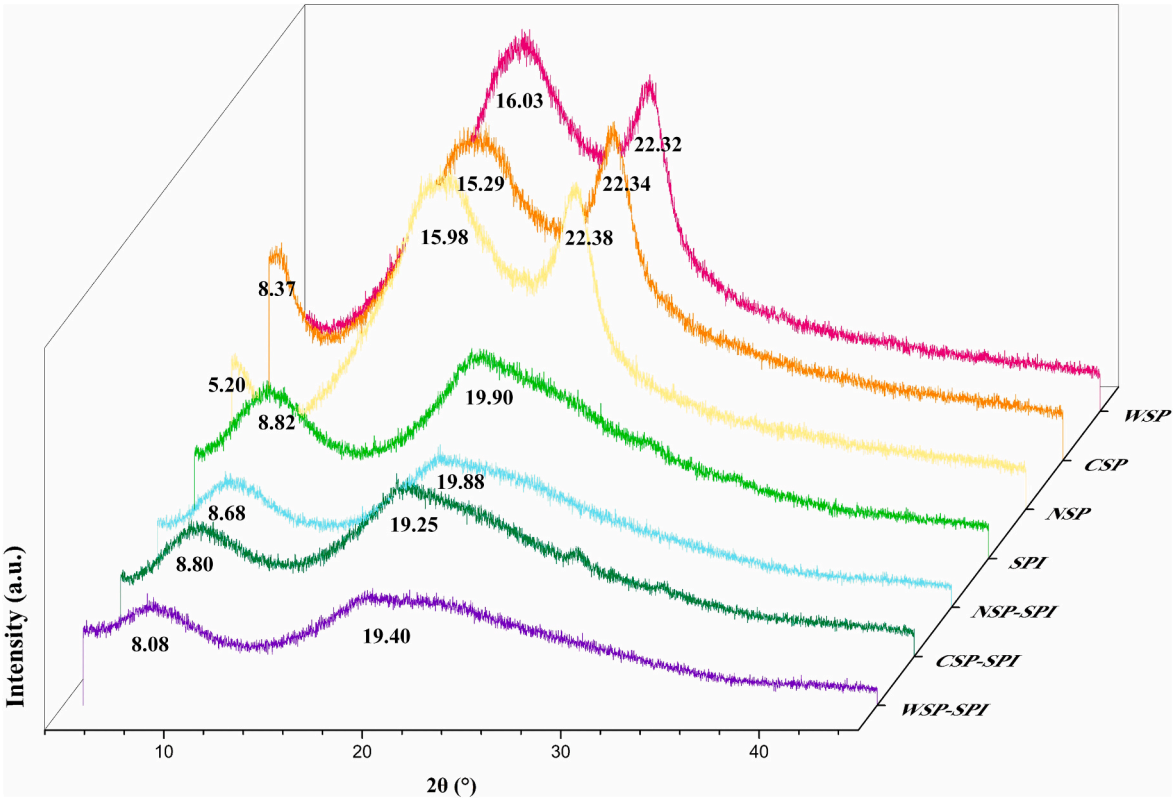

Fig. 7. X-ray diffraction of SPI, three pectin fractions and pectin-SPI gels.

3.7. Chemical forces of pectin-SPI gels

The extent of molecular interaction forces could be indirectly assessed by analyzing the amount of solubilized protein [32]. The strengthened molecular forces always accompanied the enhanced stability of gel system. Pectin fractions significantly influenced the chemical forces in pectin-SPI gels. Hydrophobic interactions were the most dominant, followed by ionic bonds (Fig. 9). Previous observations also suggested that hydrophobic interaction between polysaccharides and protein was the most primary molecular force in complex gels [32,47,48]. CSP-SPI showed the highest hydrophobic interaction (17.66 mg/mL) and ionic bond (8.55 mg/mL), which played a crucial role in the formation of a stable gel network [32]. Additionally, CSP with low methoxy enhanced salt bridges, namely "pectin-Ca-protein cross-linking" in CSP-SPI gel, as well as induced conformational changes in the gel structure [48], contributing to the formation of ionic bond. Moreover, NSP-SPI with the highest disulfide bond (6.33 mg/mL) showed in the alteration of water state, namely free water transferred to immobilized water [32], which was correlated with the improved and compact gel network. The lowest hydrogen bond was displayed in WSP-SPI. Meanwhile, NSP-SPI depicted the highest hydrogen bond (4.06 mg/mL), followed by CSP-SPI (3.59 mg/mL), no significant differences were found between them. It could be deduced that CSP and NSP easily formed cross-links with SPI through intermolecular hydrogen bonds, which was consistent with the FT-IR results.

3.8. Molecular docking

Aiming to understand the interactions between ligands and proteins [49], molecular docking has been widely used to predict the primary binding modalities between a ligand and a protein with a known three-dimensional structure. Since 7S (β-conglycinin) and 11S (glycinin) account for about 70 % of SPI, the docking simulations were performed between galacturonan and 7S and 11S [49]. The docking results and binding affinity energy were obtained in Fig. 10a. The negative binding affinity energy indicated the possibility of stable binding [49]. For the β-conglycinin component, the key interactions involved active amino acid sites ASP-137 and GLN-147 with the −6.8 kcal/mol bonding energy. The crystal binding energy and the best binding sites of galacturonan to glycinin were found to be −5.9 kcal/mol and ARG-110, respectively. These results demonstrated the smaller binding energy of galacturonan to β-conglycinin compared with glycinin, which suggested the readily bound between pectin backbone and 7S. Hydrogen bond with bond distances under 3 Å was the main interaction force for SPI and pectin main chain, which led to the stable and compact pectin-SPI gels. This was confirmed by the SPI-rice starch complex [50].

Based on the analysis of SEM, chemical forces and molecular docking, a schematic model was proposed to explain the formation of pectin-SPI gels (Fig. 10b). Hydrophobic interaction, ionic bonding, disulfide bonding and hydrogen bonding were found between pectin and SPI, which was supported by the unfolding of SPI with, the complete cross-linking of SPI. Electrostatic interactions occurred between the negative charge on the pectin side chain and the positive charge on the SPI, which also enhanced this interaction. Additionally, pectin fractions as a filler could penetrate in the gel network, resulting in the pectin-SPI composite gels with a three-dimensional complex network structure. The interactions between WSP and SPI displayed a loosely organized network, suggesting a less dense binding pattern, characterized by scattered and sparse linkages. This loosely organized interaction implied weaker binding forces or more dynamic interactions within the composite. Conversely, interactions between CSP and SPI presented an organized and dense network, with regular and strong connections indicative of strong bonding sites. This could be explained by the ionic interaction potential of CSP with the strong capability of forming cross-linked structures. The structure of NSP-SPI gel structure depicted a compact and tightly packed arrangement with less regular pattern. This suggested not only lots of frequent bonding sites but also a flexible structure in NSP that could adapt to different environmental conditions.

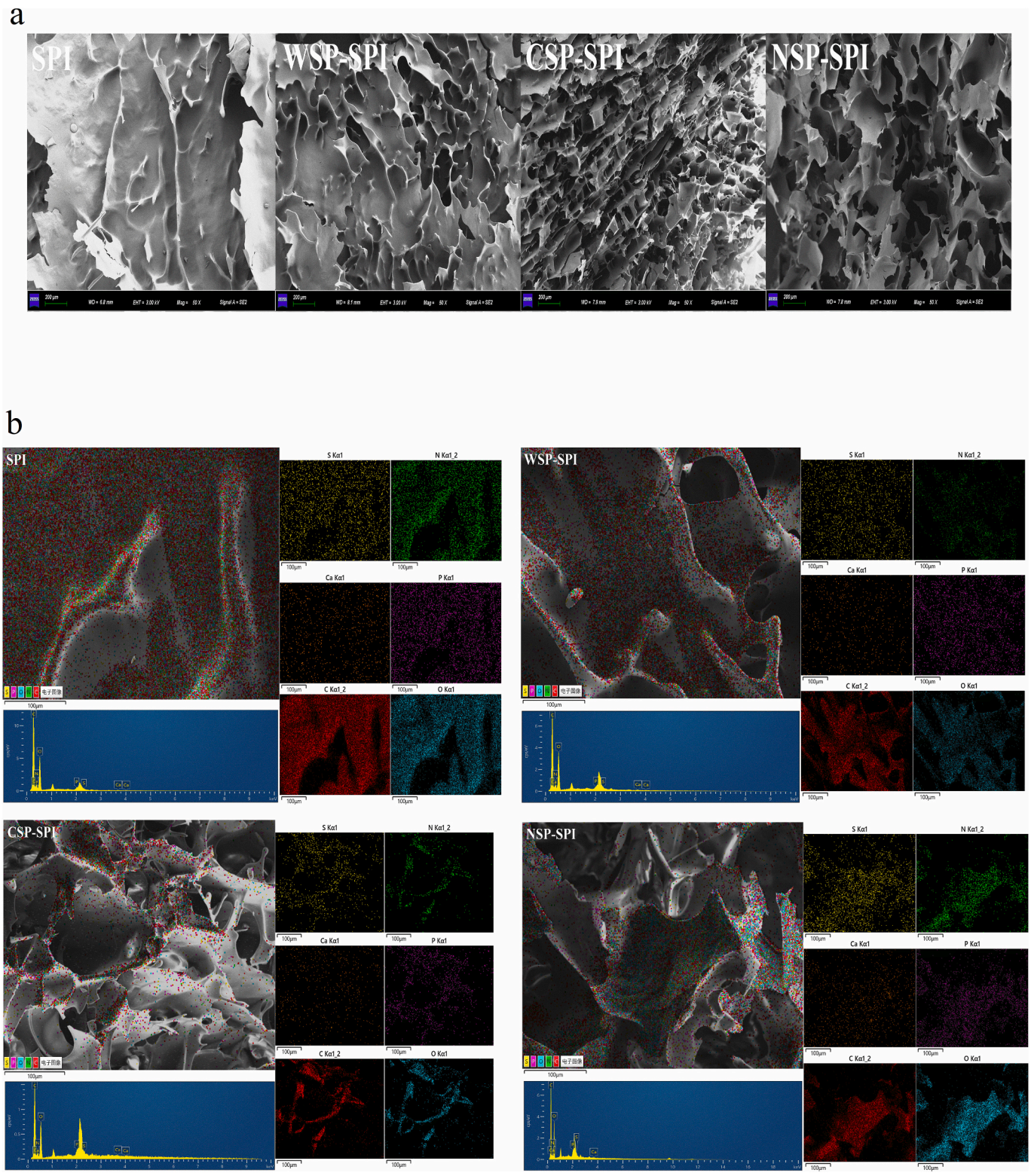

Fig. 8. Images of scanning electron microscopy (SEM) (a) and SEM-dispersive x-ray spectroscopy (b) of SPI and pectin-SPI gels.

4. Conclusion

This study gave a comprehensive understanding of the effect of pectin fractions (WSP, CSP, NSP) with distinct structure properties on the characteristics of the pectin-SPI composite gels. WSP, with high esterification, was characterized by a rich RG-I region and a large MW. while CSP, with low esterification, exhibited a high linearity and a low MW. NSP, characterized by its low linearity and high polydispersity, contributed to the abundance of side chains. Spectroscopic and microscopic analyses, including FT-IR, XRD, SEM and SEM-EDX, confirmed the formation of complex networks between pectin and SPI. Following the mixing strategy of SPI and pectin, we observed the improved viscoelastic properties (increased G′ and G″), reduced particle size, and the uniform particle distribution, which were primarily driven by

Table 4
Element percentage of SPI and pectin-SPI gels.

Atomic percentage (%)						
Elements	C	O	N	S	Ca	P
SPI	63.59	21.23	14.62	0.21	0.28	0.06
WSP-SPI	62.86	22.79	13.61	0.35	0.09	0.3
CSP-SPI	62.45	20.09	15.27	0.55	0.15	0.63
NSP-SPI	59.15	25.05	15.11	0.3	0.03	0.35

hydrophobic and ionic interactions. C, O, and N were predominant in the gel framework. Molecular docking revealed that pectin's galacturonan binds more readily to 7S than 11S due to stronger binding affinities and closer hydrogen bonds. Notably, CSP-SPI with a dense and complex network might be suitable for producing special foods with a required high firmness and stability, like plant-based meat. In contrast, the improved solubility and particle dispersion in WSP-SPI would support the applications in clear solutions, such as beverages. NSP-SPI with highest apparent viscosity that could against the external vibrations and

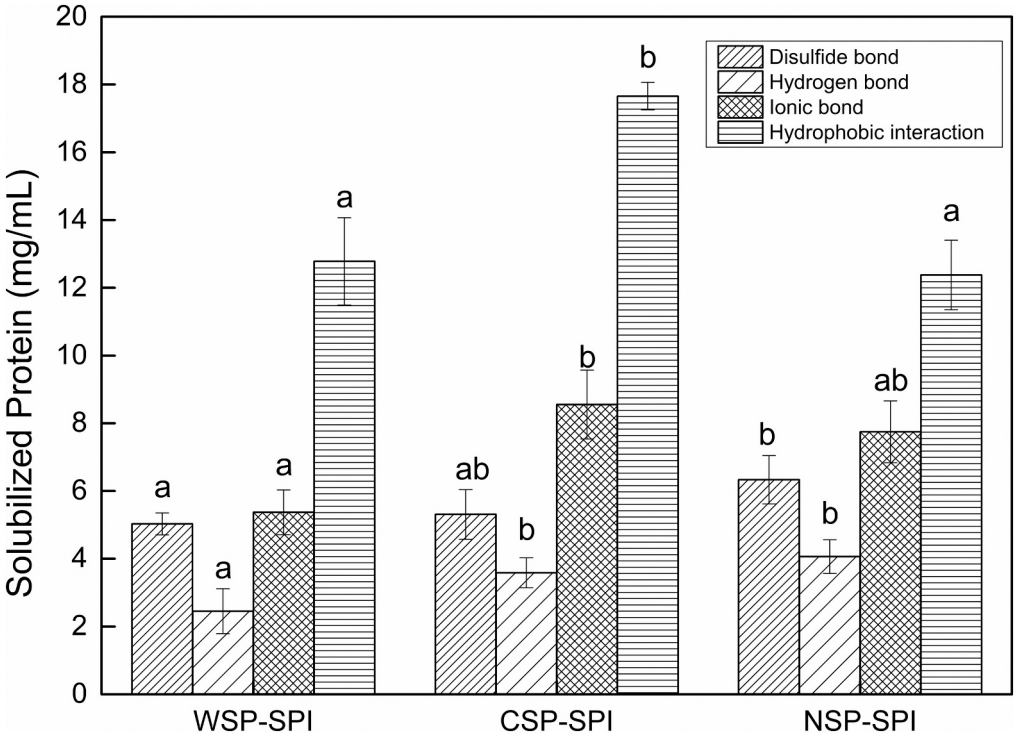

Fig. 9. Chemical forces of pectin-SPI gels.
Note: Different lowercase letters indicate significant differences among treatments ($p < 0.05$).

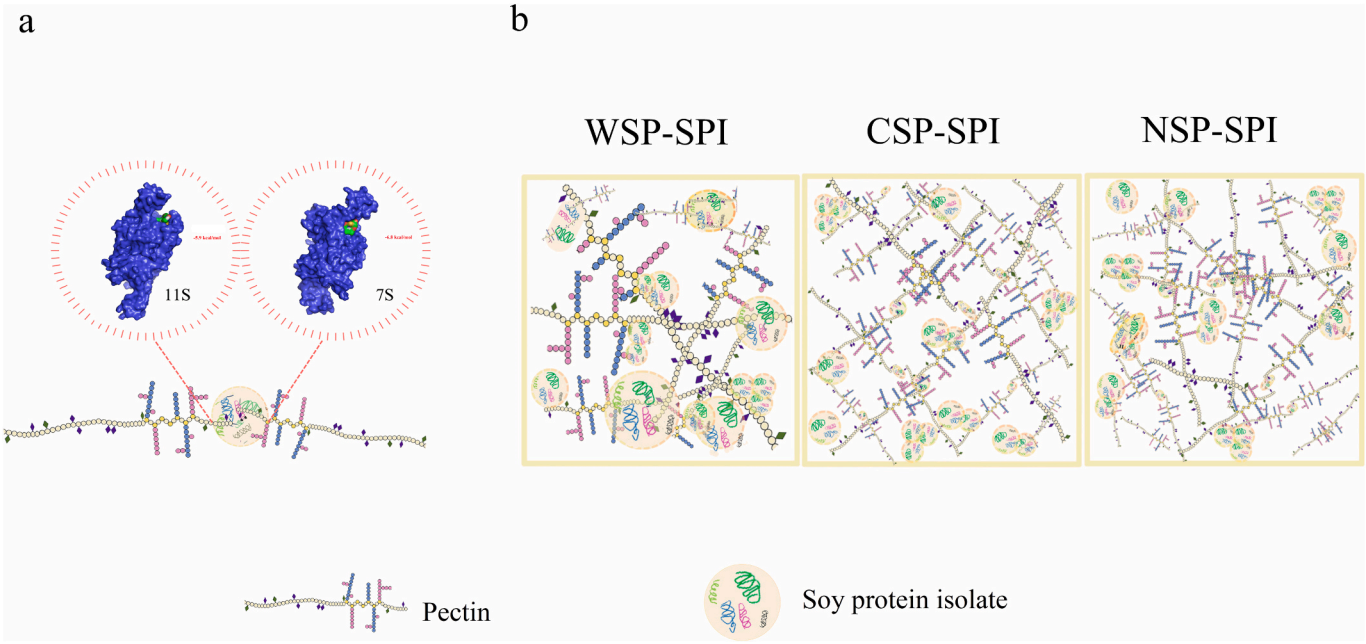

Fig. 10. Interaction and docking models between pectin and SPI (a); Schematic representation of WSP-SPI, CSP-SPI and NSP-SPI gels (b).

shear forces was preferred for products with good spread ability, like ketchup. Thus, these findings shed light on how the structural properties of pectin fractions influence gel formation mechanisms, which would provide important guidance for improving and designing new bio-composite food formulations.

CRediT authorship contribution statement

Jin Xie: Writing – original draft, Visualization, Methodology, Investigation, Data curation, Conceptualization. **Jinfeng Bi:** Supervision, Project administration, Funding acquisition. **Nicolas Jacquet:** Writing – review & editing. **Christophe Blecker:** Writing – review & editing. **Shuhan Feng:** Writing – review & editing, Formal analysis. **Xiaoxian Liu:** Data curation. **Jian Lyu:** Writing – review & editing, Supervision, Project administration.

Declaration of competing interest

The authors declared that they have no conflicts of interest to this work. We declare that we do not have any commercial or associative interest that represents a conflict of interest in connection with the work submitted.

Acknowledgments

The research was supported by the Agriculture Research System of China (CARS-30-5-02) and China Scholarship Council (202203250073).

References

[1] X. Ma, T. Yan, F. Hou, W. Chen, S. Miao, D. Liu, Formation of soy protein isolate (SPI)-citrus pectin (CP) electrostatic complexes under a high-intensity ultrasonic field: linking the enhanced emulsifying properties to physicochemical and structural properties, Ultrason. Sonochem. 59 (2019) 104748, https://doi.org/10.1016/j.ultsonch.2019.104748.

[2] A.M. Roque, D. Montinola, L. Geonzon, S. Matsukawa, C.F.Y. Lobarbio, E. B. Taboada, R.G. Bacabac, Rheological elucidation of the viscoelastic properties and network interaction of mixed high-methoxyl pectin and kappa-carrageenan gels, Food Hydrocoll. 129 (2022) 107647, https://doi.org/10.1016/j.foodhyd.2022.107647.

[3] S. Christiaens, S. Van Buggenhout, K. Houben, Z. Jamsazzadeh Kermani, K. R. Moelants, E.D. Ngouemazong, A. Van Loey, M.E. Hendrickx, Process-structure-function relations of pectin in food, Crit. Rev. Food Sci. Nutr. 56 (6) (2016) 1021–1042, https://doi.org/10.1080/10408398.2012.753029.

[4] B.M. Yapo, Pectic substances: from simple pectic polysaccharides to complex pectins—a new hypothetical model, Carbohydr. Polym. 86 (2) (2011) 373–385, https://doi.org/10.1016/j.carbpol.2011.05.065.

[5] F. Wang, J. Lyu, J. Xie, J. Bi, Texture formation of dehydrated yellow peach slices pretreated by osmotic dehydration with different sugars via cell wall pectin polymers modification, Food Hydrocoll. 134 (2023) 108080, https://doi.org/10.1016/j.foodhyd.2022.108080.

[6] V. Singh, N. Guizani, A. Al-Alawi, M. Claereboudt, M.S. Rahman, Instrumental texture profile analysis (TPA) of date fruits as a function of its physico-chemical properties, Ind. Crop. Prod. 50 (2013) 866–873, https://doi.org/10.1016/j.indcrop.2013.08.039.

[7] L. Billy, E. Mehinagic, G. Royer, C.M.G.C. Renard, G. Arvisenet, C. Prost, F. Jourjon, Relationship between texture and pectin composition of two apple cultivars during storage, Postharvest Biol. Technol. 47 (3) (2008) 315–324, https://doi.org/10.1016/j.postharvbio.2007.07.011.

[8] A.G.J. Voragen, G.-J. Coenen, R.P. Verhoef, H.A. Schols, Pectin, a versatile polysaccharide present in plant cell walls, Struct. Chem. 20 (2) (2009) 263–275, https://doi.org/10.1007/s11224-009-9442-z.

[9] F. Naqash, F.A. Masoodi, S.A. Rather, S.M. Wani, A. Gani, Emerging concepts in the nutraceutical and functional properties of pectin-a review, Carbohydr. Polym. 168 (2017) 227–239, https://doi.org/10.1016/j.carbpol.2017.03.058.

[10] J. Chen, H. Sun, T. Mu, C. Blecker, A. Richel, G. Richard, N. Jacquet, E. Haubruge, D. Goffin, Effect of temperature on rheological, structural, and textural properties of soy protein isolate pastes for 3D food printing, J. Food Eng. 323 (2022) 110917, https://doi.org/10.1016/j.jfoodeng.2021.110917.

[11] J. Xie, J. Bi, J. Nicolas, B. Christophe, F. Wang, J. Lyu, Dysphagia food: impact of soy protein isolate (SPI) addition on textural, physicochemical and microstructural properties of peach complex gels, Food Hydrocoll. 154 (2024) 110130, https://doi.org/10.1016/j.foodhyd.2024.110130.

[12] Q. Zhang, Y. Zhou, W. Yue, W. Qin, H. Dong, T. Vasanthan, Nanostructures of protein-polysaccharide complexes or conjugates for encapsulation of bioactive compounds, Trends Food Sci. Technol. 109 (2021) 169–196, https://doi.org/10.1016/j.tifs.2021.01.026.

[13] X. Ma, F. Hou, H. Zhao, D. Wang, W. Chen, S. Miao, D. Liu, Conjugation of soy protein isolate (SPI) with pectin by ultrasound treatment, Food Hydrocoll. 108 (2020), https://doi.org/10.1016/j.foodhyd.2020.106056.

[14] Y. Lan, B. Chen, J. Rao, Pea protein isolate–high methoxyl pectin soluble complexes for improving pea protein functionality: effect of pH, biopolymer ratio and concentrations, Food Hydrocoll. 80 (2018) 245–253, https://doi.org/10.1016/j.foodhyd.2018.02.021.

[15] Z. He, C. Liu, J. Zhao, W. Li, Y. Wang, Physicochemical properties of a ginkgo seed protein-pectin composite gel, Food Hydrocoll. 118 (2021), https://doi.org/10.1016/j.foodhyd.2021.106781.

[16] Q. Yu, X. Li, J. Hu, W. Wang, J. Bi, The effect of three pectin fractions variation on the browning of different dried apple products, Food Hydrocoll. 134 (2023), https://doi.org/10.1016/j.foodhyd.2022.108052.

[17] C.-l. Wu, J.-r. Qi, J.-s. Liao, Z.-w. Liu, C.-a. He, Study on low methoxyl pectin (LMP) with varied molecular structures cross-linked with calcium inducing differences in the gel properties, Food Hydrocoll. 146 (2024). doi:https://doi.org/10.1016/j.foodhyd.2023.109271.

[18] M. Zhou, J. Bi, J. Chen, R. Wang, A. Richel, Impact of pectin characteristics on lipid digestion under simulated gastrointestinal conditions: comparison of water-soluble pectins extracted from different sources, Food Hydrocoll. 112 (2021), https://doi.org/10.1016/j.foodhyd.2020.106350.

[19] C.J.F. Souza, E.E. Garcia-Rojas, Effects of salt and protein concentrations on the association and dissociation of ovalbumin-pectin complexes, Food Hydrocoll. 47 (2015) 124–129, https://doi.org/10.1016/j.foodhyd.2015.01.010.

[20] J. Xie, J. Lyu, F. Wang, L. Bai, J. Bi, Characterization of fruit pulp-soy protein isolate (SPI) complexes: effect of superfine grinding, J. Food Sci. 89 (2) (2024) 1127–1142, https://doi.org/10.1111/1750-3841.16911.

[21] J. Sun, X. Li, X. Xu, G. Zhou, Influence of various levels of flaxseed gum addition on the water-holding capacities of heat-induced porcine myofibrillar protein, J. Food Sci. 76 (3) (2011) C472–C478, https://doi.org/10.1111/j.1750-3841.2011.02094.x.

[23] S. Mallakpour, N. Mohammadi, Development of sodium alginate-pectin/TiO(2) nanocomposites: antibacterial and bioactivity investigations, Carbohydr. Polym. 285 (2022) 119226, https://doi.org/10.1016/j.carbpol.2022.119226.

[24] H. Shi, T. Zhou, X. Wang, Y. Zou, D. Wang, W. Xu, Effects of the structure and gel properties of myofibrillar protein on chicken breast quality treated with ultrasound-assisted potassium alginate, Food Chem. 358 (2021) 129873, https://doi.org/10.1016/j.foodchem.2021.129873.

[25] B. Zhang, J. Zhang, X. Yu, J. Peng, L. Pan, K. Tu, Evaluation of the adsorption capacity and mechanism of soy protein isolate for volatile flavor compounds: role of different oxygen-containing functional groups, Food Chem. 386 (2022) 132745, https://doi.org/10.1016/j.foodchem.2022.132745.

[26] J. Cui, L. Zhang, J. Wang, S. Zhao, C. Zhao, D. Liu, W. Li, J. Zheng, Study on the relationship between primary structure/ spatial conformation and gel properties of pectins from different varieties, Food Hydrocoll. 144 (2023), https://doi.org/10.1016/j.foodhyd.2023.109055.

[27] X. Ma, D. Wang, W. Chen, B.B. Ismail, W. Wang, R. Lv, T. Ding, X. Ye, D. Liu, Effects of ultrasound pretreatment on the enzymolysis of pectin: kinetic study, structural characteristics and anti-cancer activity of the hydrolysates, Food Hydrocoll. 79 (2018) 90–99, https://doi.org/10.1016/j.foodhyd.2017.12.008.

[28] X. Ma, W. Chen, T. Yan, D. Wang, F. Hou, S. Miao, D. Liu, Comparison of citrus pectin and apple pectin in conjugation with soy protein isolate (SPI) under controlled dry-heating conditions, Food Chem. 309 (2020) 125501, https://doi.org/10.1016/j.foodchem.2019.125501.

[29] J. Lyu, X. Yu, F. Wang, J. Xie, J. Bi, Cell wall modifications during storage: changes in the texture behavior of the canned yellow peach, Innov. Food Sci. Emerg. Technol. 91 (2024) 103549, https://doi.org/10.1016/j.ifset.2023.103549.

[30] L.C. Sow, N.Z.Y. Toh, C.W. Wong, H. Yang, Combination of sodium alginate with tilapia fish gelatin for improved texture properties and nanostructure modification, Food Hydrocoll. 94 (2019) 459–467, https://doi.org/10.1016/j.foodhyd.2019.03.041.

[31] A. Archut, C. Rolin, S. Drusch, H. Kastner, Interaction of sugar beet pectin and pea protein: impact of neutral sugar side chains and acetyl groups, Food Hydrocoll. 138 (2023), https://doi.org/10.1016/j.foodhyd.2022.108454.

[32] X. Ran, H. Yang, Promoted strain-hardening and crystallinity of a soy protein-konjac glucomannan complex gel by konjac glucomannan, Food Hydrocoll. 133 (2022), https://doi.org/10.1016/j.foodhyd.2022.107959.

[33] H. Chen, J. Gan, A. Ji, S. Song, L. Yin, Development of double network gels based on soy protein isolate and sugar beet pectin induced by thermal treatment and laccase catalysis, Food Chem. 292 (2019) 188–196, https://doi.org/10.1016/j.foodchem.2019.04.059.

[34] T. Cheng, Z. Wang, F. Sun, H. Liu, J. Liu, Z. Guo, L. Zhou, Gel properties of rice proteins-pectin composite and the delivery potential for curcumin: based on different concentrations and the degree of esterification of pectin, Food Hydrocoll. 146 (2024), https://doi.org/10.1016/j.foodhyd.2023.109305.

[35] J. Yi, C. Gan, Z. Wen, Y. Fan, X. Wu, Development of pea protein and high methoxyl pectin colloidal particles stabilized high internal phase pickering emulsions for β-carotene protection and delivery, Food Hydrocoll. 113 (2021), https://doi.org/10.1016/j.foodhyd.2020.106497.

[36] N.S. Said, I.F. Olawuyi, W.Y. Lee, Pectin hydrogels: gel-forming behaviors, mechanisms, and food applications, Gels 9 (9) (2023), https://doi.org/10.3390/gels9090732.

[37] Y. Mao, M. Huang, J. Bi, D. Sun, H. Li, H. Yang, Effects of kappa-carrageenan on egg white ovalbumin for enhancing the gelation and rheological properties via electrostatic interactions, Food Hydrocoll. 134 (2023), https://doi.org/10.1016/j.foodhyd.2022.108031.

[38] O.G. Jones, D.J. McClements, Stability of biopolymer particles formed by heat treatment of β-lactoglobulin/beet pectin electrostatic complexes, Food Biophys. 3 (2) (2008) 191–197, https://doi.org/10.1007/s11483-008-9068-5.
[39] F. Meng, J. Li, C. Yang, M. Wang, X. Liu, Rheological and tribological properties of high internal phase emulsions stabilized by pH-induced soy protein isolate-carrageenan complex coacervates, Food Hydrocoll. 146 (2024), https://doi.org/10.1016/j.foodhyd.2023.109191.
[40] L. Jiang, Y. Ren, Y. Xiao, S. Liu, J. Zhang, Q. Yu, Y. Chen, J. Xie, Effects of Mesona chinensis polysaccharide on the thermostability, gelling properties, and molecular forces of whey protein isolate gels, Carbohydr. Polym. 242 (2020) 116424, https://doi.org/10.1016/j.carbpol.2020.116424.
[41] X.-f. Cheng, M. Zhang, B. Adhikari, M.N. Islam, Effect of power ultrasound and pulsed vacuum treatments on the dehydration kinetics, distribution, and status of water in osmotically dehydrated strawberry: a combined NMR and DSC study, Food Bioprocess Technol. 7 (10) (2014) 2782–2792. doi:https://doi.org/10.1007/s11947-014-1355-1.
[42] L. Jiang, J. Zhang, Y. Ren, M. Shen, Q. Yu, Y. Chen, H. Zhang, J. Xie, Acid/alkali shifting of Mesona chinensis polysaccharide-whey protein isolate gels: characterization and formation mechanism, Food Chem. 355 (2021) 129650, https://doi.org/10.1016/j.foodchem.2021.129650.
[43] W. Wang, Protein aggregation and its inhibition in biopharmaceutics, Int. J. Pharm. 289 (1) (2005) 1–30, https://doi.org/10.1016/j.ijpharm.2004.11.014.
[44] H. Xue, T. Han, G. Zhang, X. Hu, R. Li, H. Liu, R. Li, Y. Tu, Y. Zhao, Combined effects of NaOH, NaCl, and heat on the characteristics of ovalbumin gel and the exploration of the mechanism of transparent gel formation, Food Hydrocoll. 140 (2023), https://doi.org/10.1016/j.foodhyd.2023.108589.
[45] S. Feng, J. Yi, Y. Ma, J. Bi, Study on the ice crystals growth under pectin gels with different crosslinking strengths by modulating the degree of amidation in HG domain, Food Chem. 428 (2023) 136758, https://doi.org/10.1016/j.foodchem.2023.136758.
[46] S. Ji, T. Xu, Y. Liu, H. Li, J. Luo, Y. Zou, Y. Zhong, Y. Li, B. Lu, Investigation of the mechanism of casein protein to enhance 3D printing accuracy of cassava starch gel, Carbohydr. Polym. 295 (2022) 119827, https://doi.org/10.1016/j.carbpol.2022.119827.
[47] M. Nakauma, T. Funami, Y. Fang, K. Nishinari, K.I. Draget, G.O. Phillips, Calcium binding and calcium-induced gelation of normal low-methoxyl pectin modified by low molecular-weight polyuronate fraction, Food Hydrocoll. 69 (2017) 318–328, https://doi.org/10.1016/j.foodhyd.2016.12.035.
[48] W. Wang, M. Shen, S. Liu, L. Jiang, Q. Song, J. Xie, Gel properties and interactions of Mesona blumes polysaccharide-soy protein isolates mixed gel: the effect of salt addition, Carbohydr. Polym. 192 (2018) 193–201, https://doi.org/10.1016/j.carbpol.2018.03.064.
[49] B. Zhang, J. Zhang, X. Yu, J. Peng, L. Pan, K. Tu, Evaluation of the adsorption capacity and mechanism of soy protein isolate for volatile flavor compounds: role of different oxygen-containing functional groups, Food Chem. 386 (2022) 132745, https://doi.org/10.1016/j.foodchem.2022.132745.
[50] N. Thirunavookarasu, S. Kumar, A. Anandharaj, A. Rawson, Enhancing functional properties of soy protein isolate—rice starch complex using ultrasonication and its characterization, Food Bioprocess Technol. (2023), https://doi.org/10.1007/s11947-023-03280-1.